

# Natural parameterized quantum circuit

Tobias Haug<sup>1,\*</sup> and M. S. Kim<sup>1</sup>

<sup>1</sup>*QOLS, Blackett Laboratory, Imperial College London SW7 2AZ, UK*

Noisy intermediate scale quantum computers are useful for various tasks including quantum state preparation, quantum metrology and variational quantum algorithms. However, the non-euclidean quantum geometry of parameterized quantum circuits is detrimental for these applications. Here, we introduce the natural parameterized quantum circuit (NPQC) with a euclidean quantum geometry. The initial training of variational quantum algorithms is substantially sped up as the gradient is equivalent to the quantum natural gradient. NPQCs can also be used as highly accurate multi-parameter quantum sensors. For a general class of quantum circuits, the NPQC has the minimal quantum Cramér-Rao bound. We provide an efficient sensing protocol that only requires sampling in the computational basis. Finally, show how to generate tailored superposition states without training. These applications can be realized for any number of qubits with currently available quantum processors.

A growing number of applications for noisy intermediate scale quantum (NISQ) computers have been proposed [1, 2] to make use of quantum computers available now and in the near future. For NISQ computers, variational quantum algorithms (VQAs) have been proposed to solve tasks difficult for classical computers [3–6] such as finding the ground state of Hamiltonians [3] or simulating quantum dynamics [7, 8]. A major obstacle for practical applications is the long training time of VQAs [9–11]. As further application, NISQ devices can serve as highly controllable quantum sensors [12–15]. However, it is unclear what is the best way to design these quantum sensors or how to efficiently sense multiple parameters at the same time [12, 16].

Parameterized quantum circuits (PQCs) are the basis of most NISQ algorithms. It is challenging to design PQCs that can efficiently run NISQ applications [17–20]. The quantum geometry of PQCs as measured by the quantum Fisher information metric (QFIM) plays a key role in this regard [17, 21, 22]. VQAs can be trained more efficiently by using the QFIM for adaptive learning rates [23] and the quantum natural gradient (QNG) [23–26]. For quantum sensing, the QFIM places a lower bound on the estimation error with the quantum Cramér-Rao bound [21, 27, 28]. However, in general the QFIM of PQCs is not characterized, requires extensive resources to be calculated [29–32] and yields a non-euclidean geometry [17], which is detrimental to tackle aforementioned tasks.

Here, we introduce the natural PQC (NPQC) which has a euclidean quantum geometry close to a particular reference parameter. This expressive NPQC can be constructed in a hardware efficient manner even for many qubits and parameters, serving as a powerful basis for various NISQ applications. The initial training iterations of VQAs with the NPQC are substantially improved as the gradient is equivalent to the QNG and we can use adaptive learning rates without calculating the QFIM. We find that the training scales favorably with increasing number of qubits which could yield an advantage on

large-scale quantum computers. We also show that the NPQC is highly useful for multi-parameter metrology and can sense many parameters efficiently at the same time with a simple protocol based on sampling in the computational basis. The NPQC promises the best accuracy for general class of PQCs with the minimal possible quantum Cramér-Rao bound. These convenient properties make the NPQC a useful basis for many other NISQ applications such as state preparation.

*Model*—The QFIM  $\mathcal{F}(\theta)$  for a PQC  $|\psi\rangle = |\psi(\theta)\rangle$  and  $M$ -dimensional parameter vector  $\theta$  is an  $M \times M$  dimensional positive semidefinite matrix [21, 28]

$$\mathcal{F}_{ij}(\theta) = 4[\langle \partial_i \psi | \partial_j \psi \rangle - \langle \partial_i \psi | \psi \rangle \langle \psi | \partial_j \psi \rangle], \quad (1)$$

where  $\partial_j |\psi\rangle$  is the gradient in respect to parameter  $\theta_j$ . The QFIM  $\mathcal{F}(\theta)$  is a metric that relates fidelity of the quantum state with the distance in parameter space  $\theta$ . When varying the parameter of the quantum state  $|\psi(\theta + d\mu)\rangle$  by a small  $d\mu$ , the fidelity is given by  $|\langle \psi(\theta) | \psi(\theta + d\mu) \rangle|^2 = 1 - \frac{1}{4} d\mu^T \mathcal{F}(\theta) d\mu$ . The variation of the distance in parameter space has a non-equal influence on the quantum state for generic PQCs with  $\mathcal{F}(\theta) \neq cI$ , where  $I$  is the identity matrix and  $c > 0$ . This non-euclidean nature of the PQC materializes in the QFIM, which acquires off-diagonal entries and non-equal diagonal entries. When the diagonal entries are non-equal  $\mathcal{F}_{ii}(\theta) \neq \mathcal{F}_{jj}(\theta)$ , then a variation of  $\theta_i$  changes the fidelity of the quantum state  $|\psi(\theta)\rangle$  by a different degree compared to  $\theta_j$ . An off-diagonal entry  $\mathcal{F}_{ij}(\theta) \neq 0$  means that a variation of parameter entries  $\theta_i$  and  $\theta_j$  lead to a change of quantum state  $|\psi(\theta)\rangle$  in non-orthogonal directions. A pictorial description of a non-euclidean fidelity landscape is shown in the upper graph of Fig.1a. When the quantum geometry is euclidean with  $\mathcal{F}(\theta) = cI$ , then all the parameters  $\theta_i, \theta_j$  are uncorrelated and they change the quantum state into orthogonal directions in the same proportional manner (see lower graph of Fig.1a). We define the NPQC as a PQC with a euclidean quantum geometry for a set of parameters.

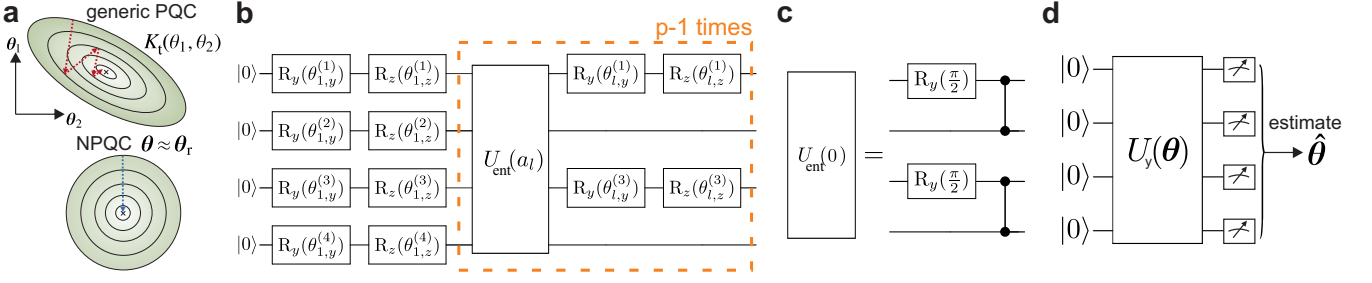


FIG. 1. **a**) The fidelity landscape  $K_t(\theta) = |\langle \psi(\theta_t) | \psi(\theta'_t) \rangle|^2$  as a function of parameter  $\theta$  of a parameterized quantum circuit (PQC). For generic PQCs, the landscape is non-euclidean and the parameters are distorted, which is characterized by the quantum Fisher information metric (QFIM)  $\mathcal{F}(\theta) \neq cI$ , where  $c > 0$  and  $I$  is the identity matrix. Training with gradient ascent (dashed line) is challenging as the gradient does not point into the optimal direction. For a natural PQC (NPQC) the fidelity landscape is euclidean with  $\mathcal{F}(\theta) = cI$ . Thus, the standard gradient points in the optimal direction, is equivalent to the quantum natural gradient (QNG) and one can use adaptive learning rates to speed up training (Eq. (6)). **b**) Hardware efficient implementation of the NPQC composed of single qubit rotations and CPHASE gates with  $N$  qubits. The NPQC has a euclidean quantum geometry close to the reference parameters  $\theta \approx \theta_r$  (Eq. (2)) with QFIM  $\mathcal{F}(\theta_r) = I$ . The reference state  $|\psi(\theta_r)\rangle$  can be extended to represent arbitrary quantum states and the NPQC is a highly expressive PQC. **c**) Example of an entangling layer  $U_{\text{ent}}(0)$  of the NPQC, consisting of  $\frac{N}{2}$  CPHASE gates and single qubit rotations. **d**) Multi-parameter quantum metrology to estimate  $\Delta\theta$  by measuring NPQC  $U_y(\theta_r + \Delta\theta)|0\rangle$  in the computational basis. The estimation error is lower bounded by the quantum Cramér-Rao bound, which is proportional to the inverse of the QFIM  $\mathcal{F}^{-1}(\theta_r) = I$ . For the NPQC, the quantum Cramér-Rao bound has the minimal value for a general class of PQCs.

A hardware efficient construction of the NPQC is shown in Fig. 1b. It consists of  $N$  qubits ( $N$  even) and  $p$  layers of unitaries  $U_l(\theta_l)$  with quantum state  $U(\theta)|0\rangle = \prod_{l=1}^p U_l(\theta_l)|0\rangle^{\otimes N}$  parameterized by the  $M$ -dimensional parameter vector  $\theta \in \mathbb{R}^M$ . The first layer consists of  $2N$  single qubit rotations around  $y$  and  $z$  axis applied on each qubit  $n$  with  $U_1 = \prod_{n=1}^N R_z^{(n)}(\theta_{1,z}^{(n)}) R_y^{(n)}(\theta_{1,y}^{(n)})$ , where  $R_\alpha^{(n)}(\theta) = \exp(-i\frac{\theta}{2}\sigma_n^\alpha)$ ,  $\alpha \in \{x, y, z\}$  and  $\sigma_n^x, \sigma_n^y, \sigma_n^z$  are the Pauli matrices applied on qubit  $n$ . Each further layer  $l > 1$  is composed of a product of two qubit entangling gates and  $N$  parameterized single qubit rotations given by  $U_l(a_l) = \prod_{k=1}^{N/2} [R_z^{(2k-1)}(\theta_{l,z}^{(2k-1)}) R_y^{(2k-1)}(\theta_{l,y}^{(2k-1)})] U_{\text{ent}}(a_l)$ , where  $U_{\text{ent}}(a_l) = \prod_{k=1}^{N/2} \text{CPHASE}(2k-1, 2k+2a_l) R_y^{(2k-1)}(\pi/2)$  and  $\text{CPHASE}(n, m)$  is the controlled  $\sigma^z$  gate applied on qubit index  $n, m$ , where indices larger than  $N$  are taken modulo. As an example, the entangling layer  $U_l(0)$  is shown in Fig. 1c. The shift factor  $a_l \in \{0, 1, \dots, N/2-1\}$  as a function of layer  $l$  is defined via the following recursive rule. Initialise the set  $A = \{0, 1, \dots, N/2-1\}$  and  $s = 1$ . In each iteration, pick and remove one element  $r$  from  $A$ . Then set  $a_s = r$  and  $a_{s+q} = a_q$  for  $q = \{1, \dots, s-1\}$ . As the last step, we set  $s = 2s$ . We repeat this procedure until no elements are left in  $A$  or the desired depth  $p$  is reached. Our construction has up to  $p_{\text{max}} = 2^{N/2}$  layers with in total  $M = N(p+1)$  parameters. The NPQC has a euclidean geometry where the QFIM is the identity for the reference parameter  $\theta_r$  given by

$$\mathcal{F}(\theta_r) = I \quad \text{for} \quad \theta_{r,l,y}^{(n)} = \pi/2, \quad \theta_{r,l,z}^{(n)} = 0. \quad (2)$$

While the euclidean geometry is exactly valid only for  $\theta_r$ ,

we find that it remains nearly euclidean in the vicinity of  $\theta \approx \theta_r$ . The QFIM  $\mathcal{F}(|\psi\rangle) = \mathcal{F}(V|\psi\rangle)$  is invariant under application of arbitrary unitaries  $V$  [21]. Thus, the euclidean quantum geometry is preserved even if we apply additional unitaries on the NPQC. We can prepare arbitrary reference states  $|\psi_r\rangle = V_{\text{ref}}|0\rangle = |\psi(\theta_r)\rangle$  with the unitary  $V_{\text{ref}}$

$$|\psi(\theta)\rangle = V_{\text{ref}} U_{\text{fix}}^\dagger U(\theta)|0\rangle, \quad (3)$$

where  $U_{\text{fix}} = U(\theta_r)$  such that  $U_{\text{fix}}^\dagger U(\theta_r) = I$ . In general the NPQC is intractable for classical computers, however for the particular case  $\theta_r$  and  $V_{\text{ref}} = I$  the NPQC is Clifford with an efficient simulation on classical computers [33]. The NPQC substantially improves various important applications of NISQ computers.

*Training VQAs*—VQAs solve tasks by optimizing the parameters  $\theta$  of the PQC in respect to a cost function. As an example, we investigate the VQA for learning the quantum state  $|\psi_t\rangle$ , an important subroutine in many VQAs [7, 8, 34, 35]. The goal is to learn the target parameters  $\theta_t = \text{argmax}_\theta K_t(\theta)$  by maximizing the fidelity

$$K_t(\theta) = |\langle \psi_t | \psi(\theta) \rangle|^2. \quad (4)$$

The cost function can be optimized by a method such as gradient ascent [3]. Here, the parameters are updated iteratively via  $\theta' = \theta + \alpha \nabla K_t(\theta)$ , where  $\alpha$  is the learning rate and  $\nabla K_t(\theta)$  is the gradient, which points in the direction of steepest change of the cost function. The NPQC can aid here by improving the learning rate  $\alpha$  and the gradient. In general PQCs, the gradient  $\nabla K_t(\theta)$  is not the best choice for optimization as it implicitly assumes that the landscape is euclidean [24, 25, 36]. As an

example, a training trajectory for a generic non-euclidean PQC is shown in the upper graph of Fig. 1a. To amend the non-euclidean nature, one can transform the gradient into the QNG ( $\mathcal{F}^{-1}(\theta) \nabla K_t(\theta)$ ) by using the inverse of the QFIM  $\mathcal{F}^{-1}(\theta)$  [24]. The QNG points in the optimal direction for gradient ascent. However, this transformation requires knowledge about the QFIM which can be difficult to acquire [24, 25, 36]. As the NPQC has a euclidean geometry close to the reference parameter ( $\mathcal{F}^{-1}(\theta_r) = I$ , Eq. (2)) by default, the gradient and QNG are equivalent

$$\nabla K_t(\theta_r) = \mathcal{F}^{-1}(\theta_r) \nabla K_t(\theta_r), \quad (5)$$

allowing us to train the first training steps in an efficient manner without the QFIM (see lower graph of Fig. 1a). To further improve training, we can replace the heuristic learning rate  $\alpha$  with adaptive learning rates that change during the training. By using the euclidean QFIM and that the fidelity takes an approximate Gaussian form, the adaptive learning rate  $\alpha_t(\theta)$  is given by (see Supplemental materials or [23])

$$\begin{aligned} \theta_1 &= \theta + \alpha_1 \nabla K_t, \quad \alpha_1 = \frac{2\sqrt{-\log(K_t(\theta))}}{\sqrt{\nabla K_t(\theta)^T \mathcal{F}(\theta) \nabla K_t(\theta)}} \\ \alpha_t(\theta) &= \frac{2}{\alpha_1 \nabla K_t(\theta)^T \mathcal{F}(\theta) \nabla K_t(\theta)} \log \left( \frac{K_t(\theta_1)}{K_t(\theta)} \right) + \frac{\alpha_1}{2}. \end{aligned} \quad (6)$$

The adaptive learning rates are chosen such that the cost function is optimized as much as possible at every iteration of gradient ascent. Both the quantum natural gradient and the adaptive learning rates can be combined to improve the first few training steps of VQAs as we know that the QFIM  $\mathcal{F}(\theta \approx \theta_r) \approx I$ . We initialise the NPQC with parameter  $\theta_r$  and choose an arbitrary initial state via Eq. (3). After a few training iterations, the parameter  $\theta$  may not be close to  $\theta_r$  anymore and the QFIM can acquire substantial off-diagonal entries. At this point we switch to heuristic learning rates. Nonetheless, improving the initial training iterations can already give us a major speed up in training VQAs.

*Metrology*— We further apply the NPQC for quantum metrology of multiple parameters (see Fig. 1d). The goal is to determine the a priori unknown  $M$ -dimensional parameter vector  $\Delta\theta$  by performing measurements on the quantum state  $|\psi(\theta_r + \Delta\theta)\rangle$ . The accuracy of estimating  $\Delta\theta$  is fundamentally limited by quantum mechanics as measured by the mean squared error  $\text{MSE}(\hat{\theta}) = \mathbb{E}(|\hat{\theta} - \theta|^2) = \text{Tr}[\text{cov}(\hat{\theta})]$ . For any quantum metrology protocol with  $n$  measurements and an unbiased estimator (i.e.  $\mathbb{E}(\hat{\theta}) = \theta$ ), the  $\text{MSE}(\hat{\theta}) \geq \frac{1}{n} \mathcal{F}^{-1}(\theta)$  is lower bounded by the inverse of the QFIM, which is called the quantum Cramér-Rao bound [21, 27, 28]. The NPQC with  $\text{Tr}[\mathcal{F}^{-1}(\theta_r)] = M$  has the smallest possible quantum Cramér-Rao bound  $Q_{\min} = M$  for a general class

of PQCs constructed from parameterized Pauli rotations and arbitrary unitaries (see Supplemental materials)

$$\text{MSE}(\hat{\theta})|_{\theta=\theta_r} \geq \frac{1}{n} \text{Tr}[\mathcal{F}^{-1}(\theta_r)] = \frac{Q_{\min}}{n} = \frac{M}{n}. \quad (7)$$

This can be intuitively understood as for a euclidean QFIM any variation of the parameters leads to an orthogonal change in the space of quantum states. Thus, each parameter direction is associated with an orthogonal quantum state that can be distinguished with a positive operator-valued measure (POVM). However, a major challenge in multi-parameter metrology is finding practical encodings and measurement settings [21, 28]. While estimating a single parameter is always possible, for multiple parameters the necessary POVMs may not commute, making it difficult to determine all parameters in a single measurement setting. Further, the POVMs may require additional resources that are not suited for NISQ devices. Using the NPQC, we can sense  $M$  parameters by sampling in the computational basis only. The setup is a modified version of the NPQC  $U_y(\theta)$ , where all the parameterized single-qubit  $z$ -rotations are removed. Then, we have the quantum state  $|\psi_y(\theta)\rangle = U_y^\dagger(\theta_r) U_y(\theta) |0\rangle$ , where we apply the adjoint  $U_y^\dagger(\theta_r)$  with parameters fixed to  $\theta_r$ . A small variation  $|\Delta\theta| \ll 1$  yields

$$|\psi_y(\theta_r + \Delta\theta)\rangle \approx \sqrt{1 - \frac{1}{4}|\Delta\theta|^2} |0\rangle + \frac{1}{2} \sum_{i=1}^M \Delta\theta_i |v_i\rangle, \quad (8)$$

where  $|v_i\rangle$  is the computational basis state with the unique number  $v_i$  for the  $i$ -th parameter of the NPQC. The number  $v_i$  can be efficiently determined on a classical computer from the gradients in respect to parameter  $\Delta\theta_i$  for the Clifford state  $|\psi_y(\theta_r)\rangle$ . The form of Eq. (8) follows from the fidelity  $K(\Delta\theta) \approx 1 - \frac{1}{4}|\Delta\theta|^2$  [21]. The absolute value of the  $i$ -th parameter entry  $|\Delta\theta_i|$  can now be estimated by sampling from  $|\psi_y(\theta_r + \Delta\theta)\rangle$  in the computational basis with  $|\Delta\theta_i| = 2\sqrt{P_i}$ , where  $P_i = |\langle\psi_y(\theta_r + \Delta\theta)|v_i\rangle|^2$  is the probability of measuring the computational basis state  $|v_i\rangle$ . For a NPQC of  $p$  layers, we can determine  $M = \frac{N}{2}(p+1)$  parameters at the same time.

*Results*— We now demonstrate the proposed applications using numerical simulations [37, 38]. In Fig. 2a, we show the performance of the VQA for learning a target quantum state  $|\psi_t\rangle$  using NPQCs. We measure the quality of the found target parameter  $\theta'_t$  with the infidelity  $\Delta K_t(\theta'_t) = 1 - K_t(\theta'_t)$ . We plot the infidelity after one iteration of gradient ascent  $\langle\Delta K_t(\theta'_t)\rangle$  using adaptive learning rates for varying initial infidelity  $\Delta K_t(\theta)$ . We compare training starting with random initial parameters of the NPQC  $\theta = \theta_{\text{rand}} \in [0, 2\pi]$  ( $\mathcal{F}(\theta_{\text{rand}}) \neq I$ ) against the reference parameter  $\theta_r$  with euclidean quantum geometry ( $\mathcal{F}(\theta_r) = I$ ). Training with  $\theta_r$  vastly outperforms the randomly chosen parameters. We numerically find that the data is fitted with

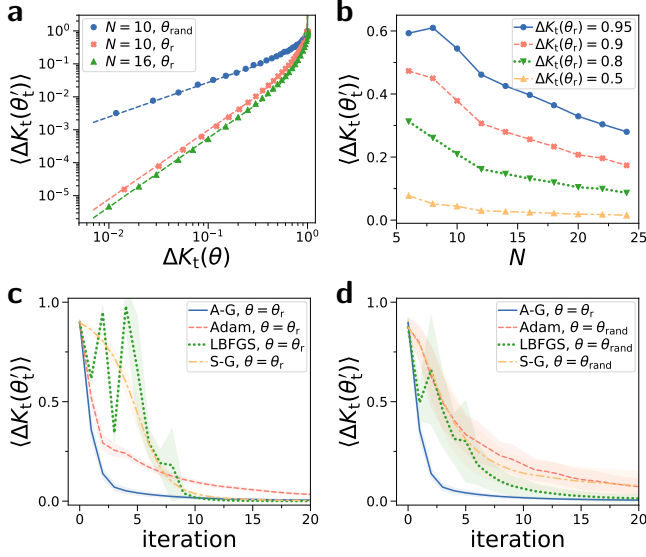


FIG. 2. **a)** Average infidelity  $\langle \Delta K_t(\theta'_t) \rangle$  after one iteration of gradient ascent with adaptive learning rates. The initial parameters of the NPQC are random  $\theta_{\text{rand}} \in [0, 2\pi]$  ( $\mathcal{F}(\theta_{\text{rand}}) \neq I$ , blue curve) or the reference parameter  $\theta_r$  ( $\mathcal{F}(\theta_r) = I$ , orange and green curves). We show  $\langle \Delta K_t(\theta'_t) \rangle$  against initial infidelity  $\Delta K_t(\theta)$ . Dashed lines are fits with  $\Delta K_t(\theta'_t) = -c \log^\nu[1 - \Delta K_t(\theta)]$  with  $\nu = 1$  for  $\theta_{\text{rand}}$  and  $\nu = 2$  for  $\theta_r$ . The scaling factors of the fits are  $c = \{6 \cdot 10^{-2}, 4.7 \cdot 10^{-3}, 2.7 \cdot 10^{-3}\}$  and number of qubits  $N = 10$ . **b)** Average infidelity after a single iteration of gradient ascent  $\langle \Delta K_t(\theta'_t) \rangle$  plotted against number of qubits  $N$  for varying infidelity before the step  $\Delta K_t(\theta_r)$ . Number of layers is  $p = 10$  and data averaged over 50 random instances. **c)** Training NPQC with initial parameter  $\theta_r$  and initial infidelity  $\Delta K_t(\theta_r) = 0.9$ . Shaded area is standard deviation of infidelity over 50 random instances of the target state. We compare adaptive gradient ascent (A-G, adaptive learning rates for first 3 iterations, then fixed learning rate  $\alpha = 0.5$ ), Adam, LBFGS and standard gradient ascent (S-G, learning rate  $\alpha = 1$ ). **d)** Compare training starting with reference parameter  $\theta_r$  against random parameter  $\theta_{\text{rand}} \in [0, 2\pi]$  with  $\Delta K_t(\theta_{\text{rand}}) = 0.9$ .

$\Delta K_t(\theta'_t) = -c \log^\nu[1 - \Delta K_t(\theta)]$ , with  $\nu = 1$  for  $\theta_{\text{rand}}$  and  $\nu = 2$  for  $\theta_r$ . In Fig. 2b for initial parameter  $\theta_r$ , we observe that the infidelity after one iteration of gradient ascent  $\langle \Delta K_t(\theta'_t) \rangle$  decreases with increasing qubit number  $N$ , demonstrating improved performance when scaling up the number of qubits of the quantum computer. In Fig. 2c, we show training with the NPQC using various optimization methods using  $\theta_r$  as initial parameter. We compare adaptive gradient ascent (A-G) with standard methods such as Adam [39], LBFGS [40] and standard gradient ascent with fixed learning rate (S-G). For adaptive gradient ascent, we use adaptive learning rates with Eq. (6) (assuming QFIM  $\mathcal{F} = I$ ) for the first three training iterations, then switch to a heuristic learning rate as the QFIM becomes non-euclidean. We find that adaptive gradient ascent performs superior compared to the others methods as the first training iterations can leverage

the euclidean quantum geometry to provide a substantial speed up. In Fig. 2d, we compare training with  $\theta_r$  as initial parameter against training with random initial parameters  $\theta_{\text{rand}} \in [0, 2\pi]$ . We find that training starting with random parameters with non-euclidean quantum geometry performs worse for all investigated optimization methods compared to training with the euclidean quantum geometry.

Now, we demonstrate our quantum metrology protocol. In Fig. 3 we show the relative root mean square error (RMSE) to estimate the  $M$ -dimensional parameter vector  $\Delta\theta$  of the NPQC. We show in Fig. 3a that the error decreases with increasing number of measurement samples  $n$ , reaching eventually a constant error. The error decreases when the parameter  $|\Delta\theta|$  to be estimated becomes smaller as we derived our protocol in the limit of small  $|\Delta\theta|$ . In Fig. 3b, we show that for infinite number of measurements  $n$  the error decreases to nearly zero with decreasing norm  $|\Delta\theta|$  of the parameter vector to be estimated. For finite  $n$ , we observe that for small  $|\Delta\theta|$  the error increases as the probability of measuring a non-zero state decreases (see Eq. (8)) and there is sweet spot where the relative error is minimal.

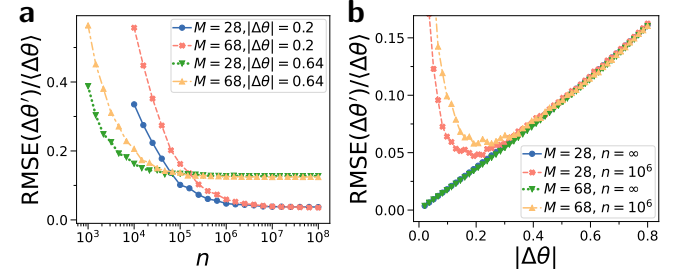


FIG. 3. **a)** Estimating parameter  $\Delta\theta$  by sampling from NPQC  $|\psi_y(\theta_r + \Delta\theta)\rangle$ . We plot the root mean square error  $\text{RMSE}(\Delta\theta') = \sqrt{\langle (\Delta\theta' - \Delta\theta)^2 \rangle}$  of the estimated parameter  $\Delta\theta'$  normalized by the average parameter  $\langle \Delta\theta \rangle$  as a function of the number of measurement samples  $n$ . We compare different numbers of parameters  $M$  and norms of parameter vector  $|\Delta\theta|$ . Data is averaged over 10 random instances of parameter  $\Delta\theta$  for  $N = 8$ . **b)** Estimation error as a function of norm of parameter vector  $|\Delta\theta|$  for different  $M$  and  $n$ .

*Discussion*— We introduced the NPQC which features a euclidean quantum geometry with QFIM  $\mathcal{F}(\theta_r) = I$  close to the reference parameter  $\theta_r$ . The reference state  $|\psi(\theta_r)\rangle$  for parameter  $\theta_r$  is completely general and can be any arbitrary quantum state while retaining its euclidean quantum geometry. We show a hardware efficient construction of the NPQC for  $M$  parameters which requires only single qubit rotations and  $(M - 2N)/2$  CPHASE gates, which can be immediately implemented on current NISQ hardware.

For VQAs, the initial training with the NPQC is vastly sped up as the gradient is by default the QNG [24] and we can use adaptive learning rates for free [23]. Train-



ing with a euclidean geometry follows an improved scaling law compared to training with a non-euclidean geometry. For the first training iteration, the infidelity with the target state decreases for increasing number of qubits. While we were only able to study up to  $N = 24$  qubits, we expect further improvements for more qubits which could be realized in current NISQ computers [41]. The NPQC could also improve the runtime of variational quantum simulation algorithms that require knowledge of the QFIM [42, 43]. When using these algorithms to study the short-time dynamics, which is close to the initial state, the QFIM is approximately the identity and we can remove the resource-heavy measurement of the QFIM from the algorithm [32].

We showed that NPQCs are accurate and practical multi-parameter quantum sensors. For a general class of circuits, NPQCs have the minimal quantum Cramér-Rao bound, which is the lower bound of the estimation error in quantum metrology [27]. In general, it is a major challenge to find practical measurement settings that are able to estimate all parameters at the same time, as the POVMs often do not commute or are not feasible to be implemented [21, 28]. We demonstrated a protocol that estimates the absolute values of  $M$  parameter entries  $\Delta\theta$  by sampling in the computational basis. The sampling can be easily done on NISQ devices and trivially commutes, allowing us to estimate all parameters in parallel. Our approach works for any number  $N$  of qubits and an extensive number  $M$  of parameters, where we can estimate  $M = \frac{N}{2}(p+1)$  parameters for  $p$  layers of entangling gates. We derived our protocol by employing a first order approximation of the parameter  $\Delta\theta$ . Our protocol becomes more accurate for small  $\Delta\theta$ , however one could derive higher order terms to improve the accuracy further. In a NISQ setting, our parameter estimation protocol can be immediately applied in atomic [44, 45] or superconducting setups [41]. The NPQC could sense an external perturbation that varies in time and space such as a magnetic field. The field induces a change in the parameters of the parameterized single qubit rotations. The parameters  $\theta_l^{(t_l)}$  of layer  $l$  provide a snapshot of the field present at time  $t_l$ . If the field varies across different qubits, we can read out the spatial variation of the field from the parameters corresponding to each qubit. As further application, one could determine calibration errors in parameterized quantum gates [46] or combine the protocol with error correction [47].

NPQCs are not limited to improving VQAs and metrology, but could be useful in other applications by utilizing its euclidean geometry. For example, one can generate tailored superposition states  $|\psi(\theta_s)\rangle = \gamma_r|\psi(\theta_r)\rangle + \gamma_t|\psi(\theta_t)\rangle + \gamma_\perp|\psi_\perp\rangle$  which are composed of reference state  $|\psi(\theta_r)\rangle$ , target state  $|\psi(\theta_t)\rangle$  and a state orthogonal to both  $|\psi_\perp\rangle$ . First, one chooses the desired fidelities of the superposition state with the reference state  $K_{r,s} = |\langle\psi(\theta_r)|\psi_s\rangle|^2$  and target state  $K_{t,s} =$

$|\langle\psi(\theta_t)|\psi_s\rangle|^2$ . Then, one can immediately calculate the parameters for the corresponding superposition state  $\theta_s$ ) (see Supplemental materials). The power to create superposition states could help to prepare basis states for quantum assisted algorithms [48–51] or become an ingredient to implement algorithms based on linear combination of unitaries on NISQ quantum computers [52, 53].

Python code for the numerical calculations are available at [54].

*Acknowledgements*— We acknowledge discussions with Kiran Khosla, Christopher Self and Alistair Smith. This work is supported by a Samsung GRC project and the UK Hub in Quantum Computing and Simulation, part of the UK National Quantum Technologies Programme with funding from UKRI EPSRC grant EP/T001062/1.

---

\* [thaug@ic.ac.uk](mailto:thaug@ic.ac.uk)

- [1] J. Preskill, *Quantum* **2**, 79 (2018).
- [2] K. Bharti, A. Cervera-Lierta, T. H. Kyaw, T. Haug, S. Alperin-Lea, A. Anand, M. Degroote, H. Heimonen, J. S. Kottmann, T. Menke, W.-K. Mok, S. Sim, L.-C. Kwek, and A. Aspuru-Guzik, arXiv:2101.08448 (2021).
- [3] A. Peruzzo, J. McClean, P. Shadbolt, M.-H. Yung, X.-Q. Zhou, P. J. Love, A. Aspuru-Guzik, and J. L. O'Brien, *Nature communications* **5**, 4213 (2014).
- [4] A. Kandala, A. Mezzacapo, K. Temme, M. Takita, M. Brink, J. M. Chow, and J. M. Gambetta, *Nature* **549**, 242 (2017).
- [5] J. R. McClean, J. Romero, R. Babbush, and A. Aspuru-Guzik, *New Journal of Physics* **18**, 023023 (2016).
- [6] M. Cerezo, A. Arrasmith, R. Babbush, S. C. Benjamin, S. Endo, K. Fujii, J. R. McClean, K. Mitarai, X. Yuan, L. Cincio, *et al.*, arXiv preprint arXiv:2012.09265 (2020).
- [7] M. Otten, C. L. Cortes, and S. K. Gray, arXiv preprint arXiv:1910.06284 (2019).
- [8] S. Barison, F. Vicentini, and G. Carleo, arXiv:2101.04579 (2021).
- [9] J. W. Z. Lau, K. Bharti, T. Haug, and L. C. Kwek, arXiv:2101.07677 (2021).
- [10] L. Bittel and M. Kliesch, arXiv:2101.07267 (2021).
- [11] C. N. Self, K. E. Khosla, A. W. Smith, F. Sauvage, P. D. Haynes, J. Knolle, F. Mintert, and M. S. Kim, arXiv:2103.16161 (2021).
- [12] J. J. Meyer, J. Borregaard, and J. Eisert, *npj Quantum Information* **7**, 1 (2021).
- [13] G. García-Pérez, M. A. C. Rossi, B. Sokolov, F. Tacchino, P. K. Barkoutsos, G. Mazzola, I. Tavernelli, and S. Maniscalco, arXiv:2104.00569 (2021).
- [14] R. Kaubruegger, D. V. Vasilyev, M. Schulte, K. Hammerer, and P. Zoller, arXiv preprint arXiv:2102.05593 (2021).
- [15] C. D. Marciniak, T. Feldker, I. Pogorelov, R. Kaubruegger, D. V. Vasilyev, R. van Bijnen, P. Schindler, P. Zoller, R. Blatt, and T. Monz, arXiv:2107.01860 (2021).
- [16] M. Szczykulska, T. Baumgratz, and A. Datta, *Advances in Physics: X* **1**, 621 (2016).
- [17] T. Haug, K. Bharti, and M. S. Kim, arXiv:2102.01659 (2021).

- [18] K. Nakaji and N. Yamamoto, arXiv:2005.12537 (2020).
- [19] S. Sim, P. D. Johnson, and A. Aspuru-Guzik, *Advanced Quantum Technologies* **2**, 1900070 (2019).
- [20] Y. Du, M.-H. Hsieh, T. Liu, and D. Tao, *Phys. Rev. Res.* **2**, 033125 (2020).
- [21] J. J. Meyer, arXiv:2103.15191 (2021).
- [22] A. Katabarwa, S. Sim, D. E. Koh, and P.-L. Dallaire-Demers, arXiv:2106.02593 (2021).
- [23] T. Haug and M. S. Kim, arXiv:2104.14543 (2021).
- [24] J. Stokes, J. Izaac, N. Killoran, and G. Carleo, *Quantum* **4**, 269 (2020).
- [25] N. Yamamoto, arXiv:1909.05074 (2019).
- [26] D. Wierichs, C. Gogolin, and M. Kastoryano, arXiv preprint arXiv:2004.14666 (2020).
- [27] C. W. Helstrom and C. W. Helstrom, *Quantum detection and estimation theory*, Vol. 84 (Academic press New York, 1976).
- [28] J. Liu, H. Yuan, X.-M. Lu, and X. Wang, *Journal of Physics A: Mathematical and Theoretical* **53**, 023001 (2019).
- [29] M. Cerezo, A. Sone, J. L. Beckey, and P. J. Coles, arXiv preprint arXiv:2101.10144 (2021).
- [30] J. Gacon, C. Zoufal, G. Carleo, and S. Woerner, arXiv:2103.09232 (2021).
- [31] J. L. Beckey, M. Cerezo, A. Sone, and P. J. Coles, arXiv:2010.10488 (2020).
- [32] B. van Straaten and B. Koczor, arXiv:2005.05172 (2020).
- [33] S. Aaronson and D. Gottesman, *Physical Review A* **70**, 052328 (2004).
- [34] M. Benedetti, D. Garcia-Pintos, O. Perdomo, V. Leyton-Ortega, Y. Nam, and A. Perdomo-Ortiz, *npj Quantum Information* **5**, 1 (2019).
- [35] J. Gibbs, K. Gili, D. Holmes, B. Commeau, A. Arrasmith, L. Cincio, P. J. Coles, and A. Sornborger, arXiv:2102.04313 (2021).
- [36] S.-i. Amari, *Information geometry and its applications*, Vol. 194 (Springer, 2016).
- [37] X.-Z. Luo, J.-G. Liu, P. Zhang, and L. Wang, *Quantum* **4**, 341 (2020).
- [38] J. R. Johansson, P. D. Nation, and F. Nori, *Computer Physics Communications* **183**, 1760 (2012).
- [39] D. P. Kingma and J. Ba, arXiv:1412.6980 (2014).
- [40] R. Fletcher, *Practical methods of optimization* (John Wiley & Sons, 2013).
- [41] F. Arute, K. Arya, R. Babbush, D. Bacon, J. C. Bardin, R. Barends, R. Biswas, S. Boixo, F. G. Brandao, D. A. Buell, *et al.*, *Nature* **574**, 505 (2019).
- [42] Y. Li and S. C. Benjamin, *Physical Review X* **7**, 021050 (2017).
- [43] X. Yuan, S. Endo, Q. Zhao, Y. Li, and S. C. Benjamin, *Quantum* **3**, 191 (2019).
- [44] H. Bernien, S. Schwartz, A. Keesling, H. Levine, A. Omran, H. Pichler, S. Choi, A. S. Zibrov, M. Endres, M. Greiner, *et al.*, *Nature* **551**, 579 (2017).
- [45] J. Zhang, G. Pagano, P. W. Hess, A. Kyprianidis, P. Becker, H. Kaplan, A. V. Gorshkov, Z.-X. Gong, and C. Monroe, *Nature* **551**, 601 (2017).
- [46] P. Cerfontaine, R. Otten, and H. Bluhm, *Physical Review Applied* **13**, 044071 (2020).
- [47] W. Górecki, S. Zhou, L. Jiang, and R. Demkowicz-Dobrzański, *Quantum* **4**, 288 (2020).
- [48] K. Bharti and T. Haug, arXiv:2011.06911 (2020).
- [49] K. Bharti and T. Haug, arXiv:2010.05638 (2020).
- [50] T. Haug and K. Bharti, arXiv:2011.14737 (2020).
- [51] K. Bharti, T. Haug, V. Vedral, and L.-C. Kwek, arXiv:2106.03891 (2021).
- [52] A. M. Childs and N. Wiebe, arXiv:1202.5822 (2012).
- [53] C. Shao, arXiv:1807.09693 (2018).
- [54] T. Haug, “Natural parameterized quantum circuit,” <https://github.com/txhaug/natural-pqc>.

## Fidelity and variance of NPQC

We define the fidelity  $K_t(\theta) = |\langle \psi_t | \psi(\theta) \rangle|^2$  of quantum state  $|\psi(\theta)\rangle$  in respect to the target state  $|\psi(\theta_t)\rangle$ . For small enough parameter distances  $\Delta\theta = \theta - \theta'$  the fidelity is approximately described by a Gaussian [23]

$$\mathcal{K}(\theta, \theta') = |\langle \psi(\theta) | \psi(\theta') \rangle|^2 \approx \exp\left[-\frac{1}{4}\Delta\theta^T \mathcal{F}(\theta) \Delta\theta\right]. \quad (9)$$

Further, the variance of the gradient is approximated by

$$\begin{aligned} \text{var}(\partial_k K_t(\theta)) &= \langle (\partial_k K_t(\theta))^2 \rangle_{\Delta\theta} - \langle \partial_k K_t(\theta) \rangle_{\theta}^2 \\ &\approx \frac{1}{M} \frac{\text{Tr}(\mathcal{F}(\theta)^2)}{\text{Tr}(\mathcal{F}(\theta))} K_t(\theta)^2 \log \left[ \frac{K_0}{K_t(\theta)} \right], \end{aligned} \quad (10)$$

where the average is first taken over distance  $\Delta\theta = \theta - \theta_t$  and then over the gradient indices  $k$ . We define  $K_0 = \max_{\theta} |\langle \psi(\theta) | \psi_t \rangle|^2$  as the maximal possible fidelity for the NPQC. For parameter  $\theta_r$ , the QFIM is given by  $\mathcal{F}(\theta_r) = I$ , resulting in simple expressions for fidelity and variance of the gradient respectively.

We now show numerical evidence for the Gaussian form of the fidelity of NPQCs. We show the fidelity as a function of distance between the reference parameter  $\theta_r$  and arbitrarily chosen target parameters  $\theta_t$   $|\Delta\theta_{r,t}|^2 = |\theta_r - \theta_t|^2$  in Fig. 4a. We observe that the data is fitted well with Eq. (9) for small distances. For larger distances, it becomes constant and reaches the fidelity  $\frac{1}{2^N}$  of Haar random quantum states. The variance of gradient is shown in Fig. 4b against  $|\Delta\theta_{r,t}|$ . We indeed find a good fit with Eq. (10). We find that the accuracy of the formulas improve with increasing number of qubits.

## Generating superposition states

The NPQC can generate superposition states of the reference state  $|\psi(\theta_r)\rangle$  and a given target state  $|\psi(\theta_t)\rangle$  with target parameters  $\theta_t$  as shown in Fig. 1c. We want to find the parameters  $\theta_s$  for the superposition state

$$|\psi_s\rangle = |\psi(\theta_s)\rangle = \gamma_r |\psi(\theta_r)\rangle + \gamma_t |\psi(\theta_t)\rangle + \gamma_{\perp} |\psi_{\perp}\rangle, \quad (11)$$

where  $|\psi_{\perp}\rangle$  is orthogonal to both reference and target states. Now, the NPQC can generate superposition states  $|\psi_s\rangle$  with tailored fidelities with the reference state  $K_{r,s} = |\langle \psi(\theta_r) | \psi_s \rangle|^2$  and the target state  $K_{t,s} = |\langle \psi(\theta_t) | \psi_s \rangle|^2$  to our choosing. We define  $\Delta\theta_{r,s} = \theta_s - \theta_r$

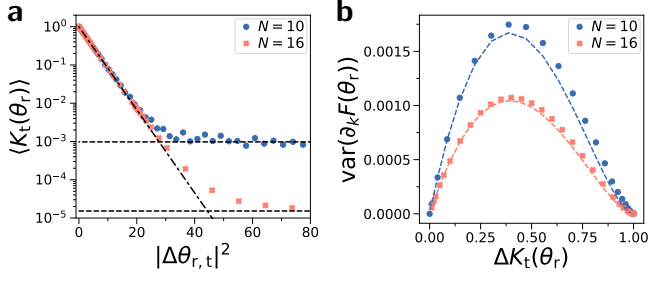


FIG. 4. **a)** Fidelity  $K_t(\theta_r)$  before optimization as a function of distance between reference and target parameters  $|\Delta\theta_{r,t}|^2$  for number of layers  $p = 10$ . Dash-dotted line is the theoretic fidelity (Eq. (9)). Dashed horizontal lines indicate fidelity of a Haar random state  $F(\theta_{\text{rand}}) = \frac{1}{2^N}$ . **b)** Variance of gradient  $\text{var}(\partial_k K_t(\theta_r))$  as a function of  $|\Delta\theta_{r,t}|$ . Dashed lines are the analytic equations for the variance (Eq. (10)).

as the difference between the parameters of the superposition state and target state, as well as  $\Delta\theta_{r,t} = \theta_t - \theta_r$  as the difference between the parameters of the target and reference state. We assume that the QFIM  $\mathcal{F} = I$ . Using (Eq. (9), [23]), we calculate the relation between fidelity and parameter distance for the reference and superposition state

$$|\Delta\theta_{r,s}|^2 = -4 \log(K_{r,s}). \quad (12)$$

For the target state and superposition state, we have

$$\begin{aligned} K_{t,s} &= e^{-\frac{1}{4}|\theta_s - \theta_t|^2} = e^{-\frac{1}{4}|\Delta\theta_{r,s} - \theta_{r,t}|^2} \\ &= e^{-\frac{1}{4}(|\Delta\theta_{r,s}|^2 + |\theta_{r,t}|^2 - 2|\Delta\theta_{r,s}||\theta_{r,t}|\cos(\angle(\Delta\theta_{r,s}, \Delta\theta_{r,t})))} \\ &= K_{r,s} e^{-\frac{1}{4}(|\theta_{r,t}|^2 - 4\sqrt{-\log(K_{r,s})}|\theta_{r,t}|\cos(\angle(\Delta\theta_{r,s}, \Delta\theta_{r,t})))}, \end{aligned}$$

where  $\angle(\Delta\theta_{r,s}, \Delta\theta_{r,t})$  is the angle between the two parameter vectors. By rearranging the equation and taking the logarithm, we finally get

$$\cos[\angle(\Delta\theta_{r,s}, \Delta\theta_{r,t})] = \frac{4 \log\left(\frac{K_{t,s}}{K_{r,s}}\right) + |\Delta\theta_{r,t}|^2}{4|\Delta\theta_{r,t}|\sqrt{-\log(K_{r,s})}}. \quad (13)$$

A solution exists when the absolute value of the right hand side of Eq. (13) is less or equal 1. The boundary of the solution space is given by

$$K_{t,s} = K_{r,s} \exp(\pm |\Delta\theta_{r,t}| \sqrt{-\log(K_{r,s})} - \frac{1}{4} |\Delta\theta_{r,t}|^2) \quad (14)$$

We define the error between desired and actual superposition state

$$\Delta C = |K_{r,s} - K'_{r,s}| + |K_{t,s} - K'_{t,s}|, \quad (15)$$

where  $K'_{r,s}$  and  $K'_{t,s}$  are the actual fidelities measured with reference and target state respectively, and  $\Delta C = 0$  corresponds to perfect creation of the desired superposition state.

Now, we investigate generating superposition states with the NPQC. The superposition state  $|\psi_s\rangle$  is a linear combination of reference state  $|\psi(\theta_r)\rangle$  and random target state  $|\psi(\theta_t)\rangle$  with infidelity between target and reference state  $\Delta K_t(\theta_r)$ . We randomly choose a desired fidelity  $K_{t,s}$  between target and superposition state, and fidelity  $K_{r,s}$  between reference and superposition state. Then, we calculate the parameters  $\theta_s$  of the superposition state using Eq. (13) and generate the state using the NPQC. In Fig. 5a, we plot the error of the superposition states  $\Delta C$  for different  $K_{t,s}$  and  $K_{r,s}$ . The dashed line shows the boundary of possible superposition states (see Supplemental materials). In Fig. 5b, we show  $\cos[\angle(\Delta\theta_{r,s}, \Delta\theta_{r,t})]$  as a function of the fidelities  $K_{r,s}$  and  $K_{t,s}$ . In Fig. 5c, we find that the error  $\Delta C$  decreases with number of parameters  $M$  of the NPQC and increases with  $\Delta K_t(\theta_r)$ .

### Gradient update

The optimal adaptive learning rates for gradient ascent [23] can be derived by using that the fidelity is approximately Gaussian for PQC. These adaptive learning rates tremendously speed up the gradient ascent algorithm. The update rule for gradient ascent is given by  $\theta_1 = \theta + \alpha_1 \nabla K_t(\theta)$  with the learning rate

$$\alpha_1 = \frac{2\sqrt{-\log(K_t(\theta))}}{\sqrt{\nabla K_t(\theta)^T \mathcal{F}(\theta) \nabla K_t(\theta)}}. \quad (16)$$

For the case where the target state cannot be represented perfectly with  $\max_{\theta} |\langle\psi(\theta)|\psi_t\rangle|^2 = K_0 < 1$ , where  $K_0$  is the maximal possible fidelity, the step has to be adjusted using  $K_t(\theta_1)$ . In this case, the parameter  $\theta'_t$  is given by  $\theta'_t = \theta + \alpha_t \nabla K_t(\theta)$ . The new adaptive learning rate is

$$\alpha_t = \frac{1}{2} \left( \frac{4}{\alpha_1 \nabla K_t(\theta)^T \mathcal{F}(\theta) \nabla K_t(\theta)} \log\left(\frac{K_t(\theta_1)}{K_t(\theta)}\right) + \alpha_1 \right). \quad (17)$$

Note the adaptive training step requires knowledge of the QFIM  $\mathcal{F}$  in general. However, for the NPQC at  $\theta_r$ , it is known that  $\mathcal{F} = I$ , where  $I$  is the identity matrix. Thus, determining the optimal learning rate is easily possible as long the parameter is close to  $\theta \approx \theta_r$ . However, for sufficient distance  $\mathcal{F}(\theta) \neq I$ , so then one has to fix the learning rate to some heuristic value.

### Performance with number of layers

In Fig. 6, we show the infidelity  $\langle\Delta K_t(\theta'_t)\rangle$  after the first training step of adaptive gradient ascent for the NPQC with initial parameter  $\theta = \theta_r$  as a function of number of layers  $p$ . We first observe an increase of  $\langle\Delta K_t(\theta'_t)\rangle$  with number of layers  $p$ , then it reaches a

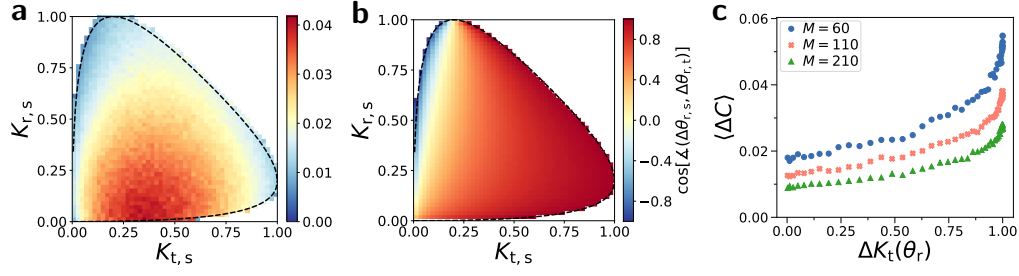


FIG. 5. **a)** Average error  $\langle \Delta C \rangle$  (Eq. (15)) of generating superposition states for  $N = 10$  qubits. We plot  $\langle \Delta C \rangle$  as a function of the desired fidelity between target and superposition state  $K_{t,s}$ , as well as reference and superposition state  $K_{r,s}$ . Dashed line is the boundary of possible superposition states. The infidelity between reference and target state is  $\Delta K_t(\theta_r) = 0.8$  and the number of parameters of the NPQC is  $M = 110$ . **a)** We show the relative angle between the difference vector of reference and superposition parameters, and reference and target parameters  $\cos[\angle(\Delta\theta_{r,s}, \Delta\theta_{r,t})]$ . **c)**  $\langle \Delta C \rangle$  as a function of infidelity  $\Delta K_t(\theta_r)$  for varying  $M$ .  $\langle \Delta C \rangle$  is averaged over 1000 random instances of fidelities  $K_{t,s}$  and  $K_{r,s}$ .

nearly constant level around  $p \approx 5$  for any  $N$  we investigated. Further increase of  $p$  yields either a further relatively smaller increase (for  $\Delta K_t(\theta_r) > \xi(N)$ ) or decrease in  $\Delta K_t(\theta'_t)$  (for  $\Delta K_t(\theta_r) < \xi(N)$ ), where we numerically find  $\xi(10) \approx 0.5$  and  $\xi(16) \approx 0.9$ .

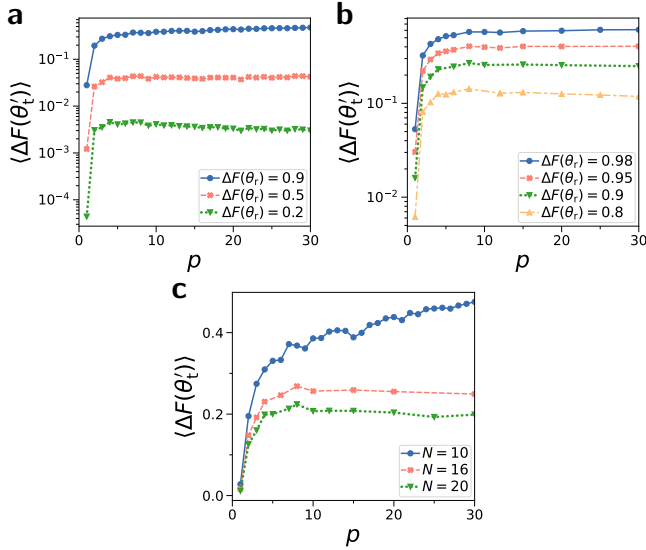


FIG. 6. **a)** We show average infidelity after optimization  $\langle \Delta K_t(\theta'_t) \rangle$  averaged over 50 random instances against number of layers  $p$  for  $N = 10$  qubits. **b)** We show infidelity for different initial infidelities  $\Delta K_t(\theta_r)$  for  $N = 16$  qubits. **c)** We show infidelity for different number of qubits  $N$  for initial infidelity  $\Delta K_t(\theta_r) = 0.9$ .

### Further training data

In Fig. 7 we show further data on training NPQCs. In Fig. 7a, we discuss the infidelity as a function of the learning rate  $\lambda$  of gradient ascent. We find that the adaptive learning rate  $\alpha_t$  (Eq. (17)) describes the best possible choice of learning rate. In Fig. 7b, we show the training

starting with  $\theta_r$  for a target state with various initial infidelities  $\Delta K_t(\theta_r)$ .

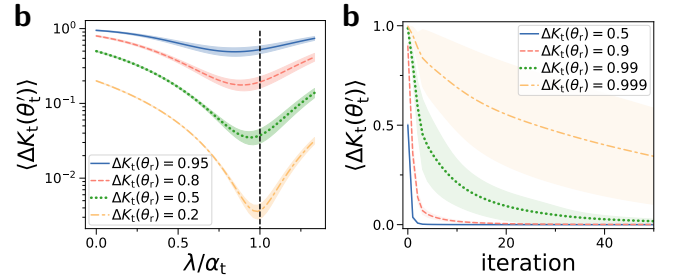


FIG. 7. **a)** Average infidelity after a gradient ascent step  $\langle \Delta K_t(\theta'_t) \rangle$  plotted against learning rate  $\lambda$  for single step of gradient ascent.  $\lambda$  is normalized in respect to analytically calculated learning rate  $\alpha_t$  (Eq. (6)), shown as vertical dashed line. Curves show various infidelity before optimization  $\Delta K_t(\theta_r)$ , with shaded area being the standard deviation of  $\Delta K_t(\theta'_t)$ . Initial state is  $|\psi(\theta_r)\rangle$ . The number of qubits is  $N = 10$  and number of layers  $p = 10$ . **b)** We show training with NPQC starting at  $\theta_r$  for different initial infidelities  $\Delta K_t(\theta_r)$ . We use adaptive learning rate for first three iterations, then use fixed learning rate  $\alpha = 0.5$ .

### Multi-parameter estimation with PQCs

We assume a general class of PQCs composed of arbitrary unitaries and Pauli rotations. We have  $|\psi(\theta)\rangle = U(\theta)|0\rangle = \prod_{l=1}^M U_l(\theta_l)|0\rangle$  given by  $M$  layers and  $M$ -dimensional parameter vector  $\theta$ . The unitary at layer  $l$  is given by  $U_l(\theta_l) = R_l(\theta_l)W_l$ , with constant  $N$ -qubit unitary  $W_l$  and a parameterized unitary  $R_l(\theta_l) = \exp(-i\frac{\theta_l}{2}P_l)$ , with parameter  $\theta_l$  and Pauli string  $P_l = \otimes_{k=1}^N \sigma_k$ , where  $\sigma \in \{\sigma^x, \sigma^y, \sigma^z, I\}$  is either a Pauli matrix or the identity. The NPQC belongs to this class of PQC as well as commonly used hardware efficient PQCs.

The quantum Fisher information metric  $\mathcal{F}$  is a  $M$ -dimensional positive semidefinite matrix given by  $\mathcal{F}_{ij}(\theta) =$



$4[\langle \partial_i \psi | \partial_j \psi \rangle - \langle \partial_i \psi | \psi \rangle \langle \psi | \partial_j \psi \rangle]$ , where  $\partial_j |\psi\rangle$  is the gradient in respect to parameter  $j$ .

The quantum Fisher information metric (via the quantum Cramér-Rao bound) sets a lower bound on the error made when using a quantum system as a sensor [21].

**Theorem 1.** *For above defined class of PQCs, the minimal possible mean squared error for the unbiased estimator  $\hat{\theta}$  is given by*

$$\text{MSE}(\hat{\theta}) \geq \frac{1}{n} \text{Tr}[\mathcal{F}^{-1}(\theta)] \geq \frac{M}{n}, \quad (18)$$

where  $n$  is the number of measurements performed.

The NPQC assumes this lower bound as  $\text{Tr}[\mathcal{F}^{-1}(\theta_r)] = M$ , making the NPQC one of the optimal sensors within above defined class of PQCs.

*Proof.* We now proceed to proof Theorem 1. The derivative acting on the unitary in layer  $l$  is given by  $\partial_i U_l = \delta_{il}(-i\frac{1}{2}P_l)U_l$ , where  $\delta_{il}$  is the Kronecker delta. We define  $U_{[l_1:l_2]} = U_{l_2} \dots U_{l_1}$ , with  $l_2 \geq l_1$  and  $|\psi_l\rangle = U_{[1:l]}|0\rangle$ . With this notation, we find  $|\partial_l \psi\rangle = U_{[l+1:M]}(\partial_l U_l)U_{[1:l-1]}|0\rangle = U_{[l+1:M]}(-i\frac{1}{2}P_l)U_l U_{[1:l-1]}|0\rangle = U_{[l+1:M]}(-i\frac{1}{2}P_l)U_{[1:l]}|0\rangle$ . We can now compute  $\langle \partial_l \psi | \partial_l \psi \rangle = \frac{1}{4}$  due to  $P_l^2 = I$  and  $\langle \psi | \partial_l \psi \rangle = -i\frac{1}{2}\langle \psi_l | P_l | \psi_l \rangle$ . The diagonal terms of the quantum Fisher information metric are then given by

$$\mathcal{F}_{ii} = 4[\langle \partial_i \psi | \partial_i \psi \rangle - \langle \partial_i \psi | \psi \rangle \langle \psi | \partial_i \psi \rangle] = 1 - (\langle \psi_i | P_i | \psi_i \rangle)^2. \quad (19)$$

Due to the eigenvalues of  $P_i$  being  $\pm 1$ , we have  $0 \leq (\langle \psi_i | P_i | \psi_i \rangle)^2 \leq 1$ . Thus, the diagonal entries  $\mathcal{F}_{ii}$  are within  $0 \leq \mathcal{F}_{ii} \leq 1$  and the trace of  $\mathcal{F}$  is upper bounded by

$$\text{Tr}(\mathcal{F}) = \sum_{i=1}^M \mathcal{F}_{ii} \leq M. \quad (20)$$

By combining Eq. (20) and Lemma 2, Eq. (18) follows immediately.  $\square$

**Lemma 2.** *Given a positive semidefinite matrix  $\mathcal{A}$  with dimension  $M \times M$ ,  $M \in \mathbb{N}$ , the trace of the inverse matrix  $\mathcal{A}^{-1}$  is lower bounded by  $\text{Tr}(\mathcal{A}^{-1}) \geq \frac{M^2}{\text{Tr}(\mathcal{A})}$ .*

*Proof.* For a sequence of numbers  $x_1, x_2, \dots, x_M$  with  $x_n \geq 0$ , the arithmetic mean is always larger than harmonic mean

$$\frac{1}{M} \sum_{n=1}^M x_n \geq \frac{M}{\sum_{n=1}^M \frac{1}{x_n}}, \quad (21)$$

which is known from the relations of the Pythagorean means. A simple calculation shows

$$\sum_{n=1}^M \frac{1}{x_n} \geq \frac{M^2}{\sum_{n=1}^M x_n}. \quad (22)$$

The positive semidefinite matrix  $A$  has only non-negative eigenvalues  $\lambda_n \geq 0$ . The trace is given by

$$\text{Tr}(\mathcal{A}) = \sum_{n=1}^M \lambda_n. \quad (23)$$

and accordingly for the inverse

$$\text{Tr}(\mathcal{A}^{-1}) = \sum_{n=1}^M \frac{1}{\lambda_n}. \quad (24)$$

Using Eq. (22), we can immediately show

$$\text{Tr}(\mathcal{A}^{-1}) \geq \frac{M^2}{\text{Tr}(\mathcal{A})}, \quad (25)$$

$\square$

Using Eq. (25) and Eq. (20), we find

$$\text{Tr}(\mathcal{F}^{-1}) \geq \frac{M^2}{\text{Tr}(\mathcal{F})} \geq M, \quad (26)$$

which we insert in Eq. (18).

### Note on extending the NPQC

While our construction of NPQC can generate an exponential number of parameters, it does not cover the full Hilbert space. However, we note that it is possible to get NPQCs with  $2^{N+1} - 2$  parameters that exactly cover all possible quantum states, however this requires an implementation with lower efficiency where in each layer there are less than  $N$  parameters.